AGU PUBLICATIONS

Geochemistry, Geophysics, Geosystems

RESEARCH ARTICLE
10.1002/2014GC005595

Key Points:
- Ge/Si ratios of late Ediacaran bedded cherts are reported
- Normal seawater is the primary Si source of the bedded chert formation
- Late Ediacaran seawater contains low concentrations of dissolved organic carbon

Correspondence to:
B. Shen,
bingshen@pku.edu.cn

Citation:
Dong, L., et al. (2015), Germanium/silicon of the Ediacaran-Cambrian Laobao cherts: Implications for the bedded chert formation and paleoenvironment interpretations, *Geochem. Geophys. Geosyst.*, *16*, doi:10.1002/2014GC005595.

Received 2 OCT 2014
Accepted 8 FEB 2015
Accepted article online 12 FEB 2015

Germanium/silicon of the Ediacaran-Cambrian Laobao cherts: Implications for the bedded chert formation and paleoenvironment interpretations

Lin Dong[1,2], Bing Shen[1], Cin-Ty A. Lee[3], Xu-jie Shu[3,4], Yang Peng[1], Yuanlin Sun[1], Zhuanhong Tang[5], Hong Rong[5], Xianguo Lang[1], Haoran Ma[1], Fan Yang[1], and Wen Guo[1]

[1]Key Laboratory of Orogenic Belts and Crustal Evolution, MOE, School of Earth and Space Science, Peking University, Beijing, People's Republic of China, [2]Laboratory of Paleontology and Stratigraphy, Nanjing Institute of Geology and Paleontology, Chinese Academy of Science, Nanjing, People's Republic of China, [3]Department of Earth Science, Rice University, Houston, Texas, USA, [4]School of Earth Science and Engineering, Nanjing University, Nanjing, People's Republic of China, [5]Guangxi Institute of Regional Geological Survey, Guilin, People's Republic of China

Abstract Sedimentary strata of the terminal Ediacaran (635–542 Ma) to early Cambrian (542–488 Ma) Laobao-Liuchapo bedded cherts in the South China Block include the Ediacaran Oxidation Event and the Cambrian explosion. Understanding the origin and depositional environment of the bedded cherts may provide insight into how the Earth's surface environment changed between the Proterozoic and Phanerozoic. We measured major and trace element compositions and Ge/Si ratios of the Laobao cherts from northern Guangxi province. The Laobao cherts were deposited in the deep basinal environment of the South China Block. We show that the composition of the Laobao cherts is determined by a mixture of four components: quartz, clay, carbonate, and pyrite/iron-oxide. The quartz component is the dominant component of the Laobao cherts. The maximum estimated Ge/Si of the quartz component is between 0.4 and 0.5 μmol/mol, which is close to the Ge/Si of modern seawater and biogenic silica but 1 order of magnitude lower than that of hydrothermal fluids. These Ge/Si systematics suggest that normal seawater rather than mid-ocean ridge hydrothermal fluids is the primary Si source for the Laobao cherts. The Ge/Si of the clay component varies between 1 and 10 μmol/mol, which is comparable to the Ge/Si of typical marine clays, but 10–100 times lower than that of chert nodules from early Ediacaran beds (the Doushantuo Formation) predating the terminal Ediacaran Laobao cherts studied here. Our observations indicate that the clay component Ge/Si ratio decreased from the early Ediacaran to the late Ediacaran. We speculate that high Ge/Si ratios in clays reflect the preferential chelation of Ge by dissolved organic compounds adsorbed onto clays. If so, this suggests that the decrease in Ge/Si ratio of the clay component in the Ediacaran signifies a decrease in the total dissolved organic carbon content of seawater toward the Ediacaran-Cambrian transition, consistent with oxidation of the oceans during the late Ediacaran. Finally, the seawater origin of the Laobao cherts also suggests that replacement of carbonate may not be the primary cause for bedded chert formation. Instead, direct precipitation from seawater or early diagenetic silicification of calcareous sediments, perhaps due to the emergence of Si-accumulation bacteria, may have been responsible for the bedded Laobao-Liuchapo chert formation in South China Block.

1. Introduction

The Ediacaran (635–542 Ma)-Cambrian (542–488 Ma) transition is a critical interval in Earth's history. During this transition, Earth experienced dramatic changes in its atmosphere, hydrosphere, and biosphere. A prerequisite for the evolution of animal life is a substantially oxygenated ocean [*Knoll*, 1996]. Recent studies indicate that atmospheric oxygen remained low (probably $<$0.1% of present atmospheric level) during the mid-Proterozoic (1.8–0.75 Ga) and that oxygenation might have begun as early as $\sim$750 Ma [*Lyons et al.*, 2014; *Planavsky et al.*, 2014; *Reinhard et al.*, 2013]. However, deep ocean oxidation might not occur until the Ediacaran Period, collectively termed the Ediacaran Oxidation Event or Neoproterozoic Oxidation Event [*Fike et al.*, 2006; *Kaufman et al.*, 2007; *McFadden et al.*, 2008; *Shields-Zhou and Och*, 2011]. The evidence cited for the oxidation of Ediacaran oceans comes from a global negative carbon isotope excursion (the Shuram excursion), interpreted to result from remineralization of dissolved organic carbon (DOC) stored in anoxic

deep oceans [*Fike et al*., 2006; *Kaufman et al*., 2007; *McFadden et al*., 2008; *Rothman et al*., 2003]. Of interest is the possibility that the initiation and the full extent of the Cambrian explosion of diversity postdated the Ediacaran Oxidation Event by more than 10 and 30 million years. For example, Ediacaran-Cambrian sediments in the South China Block (SCB) show that the negative carbon isotope excursion in the Doushantuo Formation (EN3) occurred before 551 Ma [*Condon et al*., 2005; *McFadden et al*., 2008; *Zhu et al*., 2013], but the Cambrian explosion began at ~541 Ma and was not complete until 521 Ma [*Shu*, 2008].

In order to understand how the oxidation of Ediacaran oceans and Cambrian explosion relate to each other, it is important to study continuous sedimentary sections that have conformable contacts with both the underlying Ediacaran and the overlying early Cambrian strata. Compared with the fossiliferous but stratigraphically incomplete carbonate/shale sequences in the platform of the SCB, formations deposited in deep water settings, like the bedded Laobao-Liuchapo cherts, continuously and conformably span these two events [*Chen et al*., 2015]. This stratigraphically complete bedded chert may provide a unique window into understanding the Ediacaran-Cambrian transition.

Two goals are pursued in this study. First, we aim to constrain the origin of Si making up the bedded cherts. Based on various major and trace element systematics as well as Si isotopes, the Si is thought to originate from normal seawater (continental weathering fluxes is the dominant Si input) or abrupt eruption of mid-ocean ridge hydrothermal fluids [*Chang et al*., 2008, 2010; *Fan et al*., 2013; *Peng et al*., 1999; *Wang et al*., 2012b; *Yang et al*., 2011; *Zhao*, 1999]. To gain further insight into the origin of the chert, we examined the germanium (Ge) and Si systematics of the Laobao cherts from northern Guangxi province, South China. Ge and Si belong to the same group in the Periodic Table and have similar chemical properties. In silicate minerals, Ge can replace Si in the crystal lattice, but the degree of substitution is mineral dependent, as exemplified by the variation of Ge/Si ratios in silicate materials (0.5–6 μmol/mol) [*Bernstein*, 1985; *Kurtz et al*., 2002]. Ge/Si is fractionated during low-temperature weathering or hydrothermal processes. Weathering of continental rocks yields riverine fluxes with lower Ge/Si ratios of ~0.4–1 μmol/mol than the bulk upper continent crust (~1.8 μmol/mol) [*Froelich et al*., 1985; *Mortlock and Froelich*, 1987; *Rudnick and Gao*, 2003], leaving weathering residues (e.g., soil) enriched in Ge [*Kurtz et al*., 2002]. In contrast, hydrothermal fluids have much higher Ge/Si ratios (~11 μmol/mol) than oceanic basalts (~2.5 μmol/mol) [*De Argollo and Schilling*, 1978; *Mortlock and Froelich*, 1986; *Mortlock et al*., 1993].

Because biogenic silica does not fractionate Ge from Si [*Froelich et al*., 1989; *Murnane and Stallard*, 1988], seawater Ge/Si ratios reflect varying proportions of hydrothermal and continental weathering fluxes. In the modern ocean, a seawater Ge/Si of ~0.72 implies that continental weathering may be the dominant Si influx (~80–90%) into the oceans [*Froelich et al*., 1989]. This estimate is broadly consistent with the predominant Si influx from continental weathering (~80%) [*Tréguer et al*., 1995]. Although it is unclear whether Ge/Si is preserved during diagenesis, linear correlation between seawater strontium isotopes and Ge/Si of Mesozoic and Cenozoic deep sea cherts suggest that Ge/Si in cherts are robust proxies [*Kolodny and Halicz*, 1988]. The second goal of this study is to use the bedded cherts as potential proxies for understanding seawater chemistry. There is geochemical evidence indicating that the Laobao-Liuchapo bedded cherts were deposited in reducing conditions. For example, enrichment in redox sensitive trace elements (U, V, Mo) with low Th/U, high V/Sc and V/(V+Ni) argues that the deposition of the Laobao chert occurred under an anoxic conditions [*Chang et al*., 2012]. Similar conclusions have been drawn from Fe speciation and sulfur isotope studies of the equivalent Liuchapo cherts deposited on the slope of the SCB [*Wang et al*., 2012a], although it is still unclear whether Fe speciation can be applied to cherts. These observations suggest that the terminal Ediacaran seawater in the deep water settings of the SCB might have remained anoxic after the hypothesized oxidation of Ediacaran ocean [*Chang et al*., 2012; *Wang et al*., 2012a]. What is unclear is whether the DOC content continued to remain high. Ge/Si systematics may provide some insight because chelation of Ge with organic compounds followed by absorption onto clay mineral surfaces can lead to clay components with high Ge/Si ratios and thus may be diagnostic of seawater with high DOC content [*Pokrovski and Schott*, 1998; *Pokrovski et al*., 2000; *Shen et al*., 2011a]. In a previous study, we examined the Ge/Si systematics of cherts from the Doushantuo formation, which formed in the early Ediacaran, predating the oxidation of Ediacaran ocean (the Shuram excursion). We showed that Ge/Si systematics were consistent with high DOC in seawater prior to the oxidation of Ediacaran ocean [*Shen et al*., 2011a]. Here we build on the use of Ge/Si systematics as a diagnostic of DOC levels in seawater by examining the Ge/Si systematics of the younger Laobao cherts to help evaluate whether high DOC oceans extended into the Ediacaran-Cambrian transition.

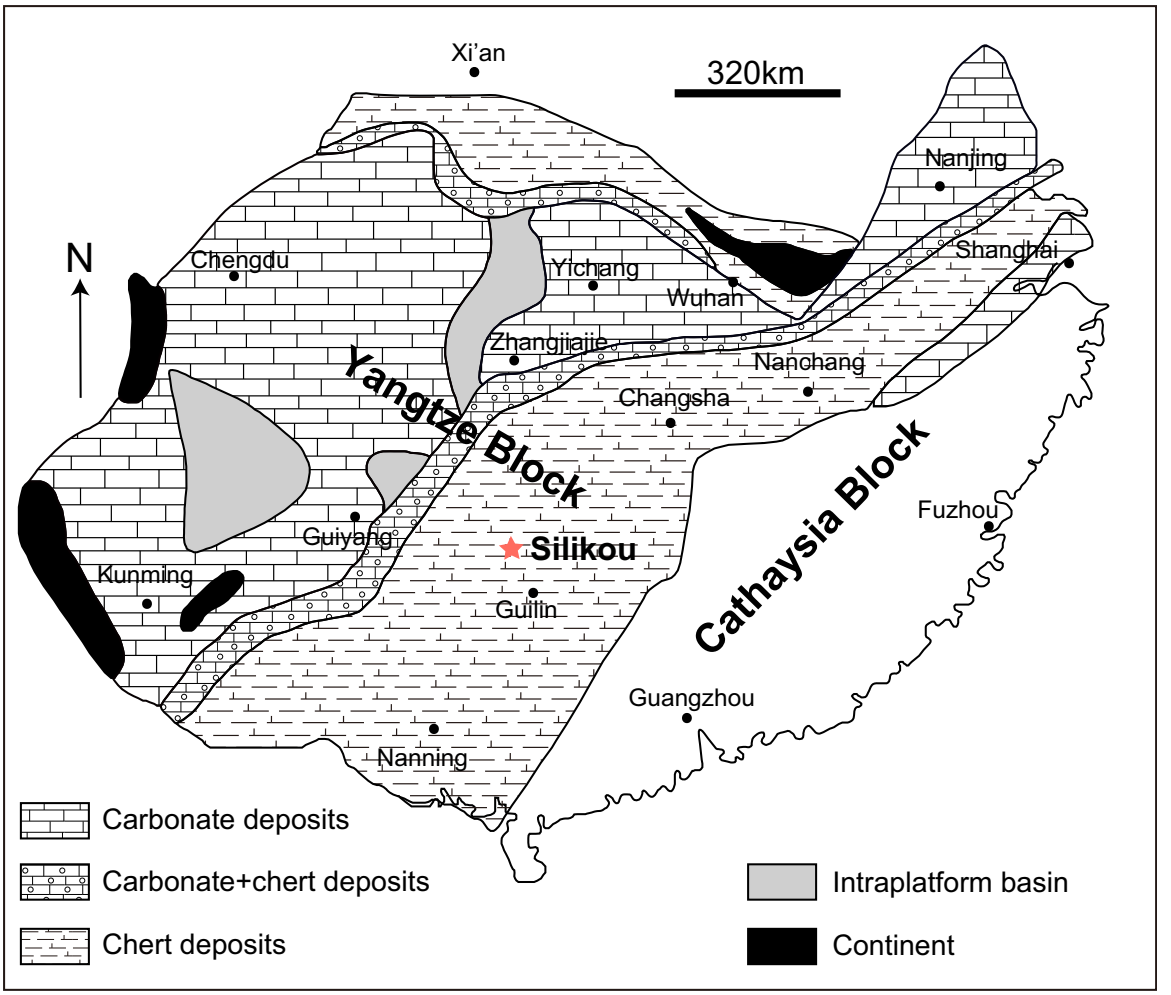

Figure 1. Paleogeographic map for SCB during the Ediacaran-Cambrian transition (modified from *Wang et al.* [2012]). Note widespread deposition of the Laobao-Liuchapo cherts in the slope and basin environment of SCB. The sampling locality is shown in red star.

2. Geological Background

Terminal Ediacaran to early Cambrian bedded chert formations are variably called the Laobao cherts in northern Guangxi province, the Liuchapo cherts in Guizhou and Hunan provinces, and the Piyuancun cherts in Anhui and Zhejiang provinces. In this paper, chert samples were collected from the Laobao Formation in the Silikou section in the Sanjiang county, northern Guangxi province (Figure 1). Paleodepositional environment reconstructions indicate that the Sanjiang area was located in deep basinal environments of the SCB [*Jiang et al.*, 2011; *Wang and Li*, 2003; *Wang et al.*, 2012b]. In the Sanjiang area, the Cryogenian (750–635Ma)-Ediacaran succession consists of, in ascending order, the Chang'an, Fulu, Lijiapo, Doushantuo, and Laobao Formations (Figure 2). The Laobao Formation conformably overlies the siltstone and mudstone of the Doushantuo Formation, and consists of black, organic-rich, thin to medium-bedded cherts (Figures 2, 3a, and 3b). Many chert layers are finely laminated (Figure 3d). The upper boundary of the Laobao Formation is marked by the presence of black shale of the early (?) Cambrian Qingxi Formation. The contact between the Laobao chert and Cambrian black shale is conformable.

The Laobao chert has traditionally been compared with the Liuchapo Formation deposited in the slope environments of SCB [*Wang et al.*, 1980]; both have been regarded as equivalent to the Dengying carbonates in the Yangtze carbonate platform [*Wang et al.*, 1984a, 1984b]. However, recent studies indicate that the upper boundaries of the Dengying Formation and the Laobao-Liuchapo cherts are not synchronous [*Amthor et al.*, 2003; *Chen et al.*, 2015; *Wang et al.*, 2012c]. The contact between the Dengying Formation and the overlying black chert-

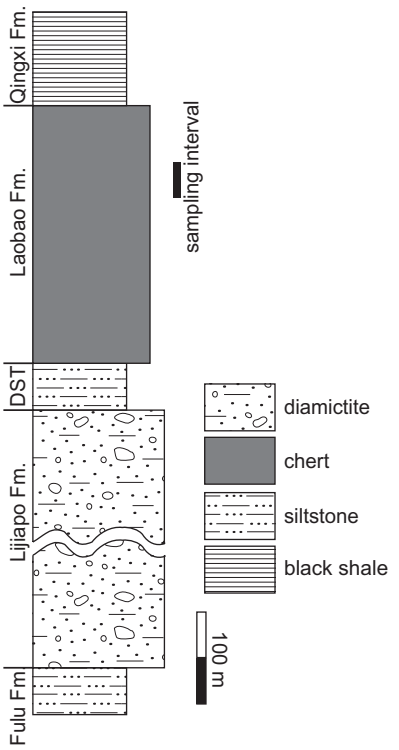

Figure 2. Stratigraphic column of the Cryogenian-Ediacaran-Cambrian succession in the Silikou section, northern Guangxi province. Sampling interval is marked against the stratigraphic column. DST: Doushantuo Formation.

phosphorite of the Yanjiahe Formation is estimated to be ~538 Ma, close to the Ediacaran-Cambrian boundary [*Amthor et al*., 2003]. However, the Laobao-Liuchapo Formation might have extended into Cambrian, and upper boundary of the Laobao-Liuchapo chert might be diachronous within the SCB [*Chen et al*., 2015; *Wang et al*., 2012b, 2012c]. Small shelly fossils recovered from the upper Liuchapo Formation are composed of a mixture of the small shelly fossil assemblage I and assemblage II, suggesting an extension to the Tommotian (534–530Ma) [*Wang et al*., 1984b]. Typical Ediacaran fossils, *Palaeopascichnus* have been reported from the Liuchapo cherts in central Guizhou province and the equivalent Piyuancun cherts in southern Anhui province [*Dong et al*., 2008, 2012]. Based on our observations, *Palaeopascichnus* occurs in the lower Laobao Formations as well (Figure 3c). The paleontological data imply that the Laobao-Liuchapo cherts were deposited from the terminal Ediacaran to early Cambrian. Thus, the Ediacaran-Cambrian boundary is located within the Laobao-Liuchapo Formation.

3. Methods

Polished thin and thick sections were prepared for petrographic observation and laser ablation inductively coupled plasma mass spectrometry (LA-ICP-MS) analyses, respectively, at Rice University (USA). Measurements were conducted at medium mass resolution ($m/\Delta m = 3000$). The following masses were monitored: ^{23}Na, ^{25}Mg, ^{27}Al, ^{30}Si, ^{31}P, ^{39}K, ^{43}Ca, ^{45}Sc, ^{48}Ti, ^{51}V, ^{52}Cr, ^{55}Mn, ^{57}Fe, ^{59}Co, ^{60}Ni, ^{63}Cu, ^{66}Zn, ^{69}Ga, ^{74}Ge, ^{89}Y, and ^{91}Zr. At medium mass resolution, all significant isobaric interferences were resolved (e.g., $^{40}Ar^{16}O^{1}H^{+}$ was resolved from ^{57}Fe). Correction of magnet drift (mass calibration) was resolved by centering on the $^{40}Ar^{40}Ar^{+}$ dimer during each run. We chose the transect mode for laser ablation. The following laser operating parameters were used: laser beam diameter of 55 μm, pulse frequency of 10 Hz, energy intensity at a ~20 J/cm^2, and at beam moving velocity of 20 μm/s. A ~30 s gas background was acquired while the laser was off, followed by ablation and acquisition of the signal. After subtracting background gas signals from sample signals, the background-corrected signals were normalized to the ^{30}Sisignal, which we used as an internal standard. External reference glass standards (United States Geological Survey basaltic glasses BHVO2g, BCR2g) were analyzed before the sequence of samples. For each sample, at least four measurements were taken from the least altered areas. Background-corrected signals were converted into elemental concentration ratios by calibration against BHVO2g and BCR2g external standards. Absolute compositions were calculated from elemental ratios and on a volatile-free basis (i.e., C, S, and H). In this treatment, all the measured major and minor elements are considered as oxides (Na_2O, MgO, Al_2O_3, SiO_2, P_2O_5, K_2O, CaO, TiO, MnO, and FeO) and then sum up to 100%. This approach has a slight systematic bias, because Ca and Mg could be in the form of carbonate and Fe could be in the form of Fe_2O_3or FeS_2. For most samples, the calculated SiO_2 contents are greater than 90%, so the volatile-free concentrations of other oxides are biased by ~5% at most. However, such bias in absolute concentrations does not apply to Ge/Si ratios. Ge/Si is expressed here in μmol/mol. Analytical uncertainties are calculated by multiple measurements of BHVO2g and BCR2g standards. The relative uncertainty of Ge/Si is better than 8% (1σ). LA-ICP-MS measurements are bulk measurements so do not differentiate between different components in the chert. However, component proportions can be estimated by multielement mass balance inversion.

4. Results

Eight Laobao chert samples were analyzed. The major and trace element compositions as well as Ge/Si (μmol/mol) are listed in Table 1. Based on major element compositions, the Laobao chert can be classified

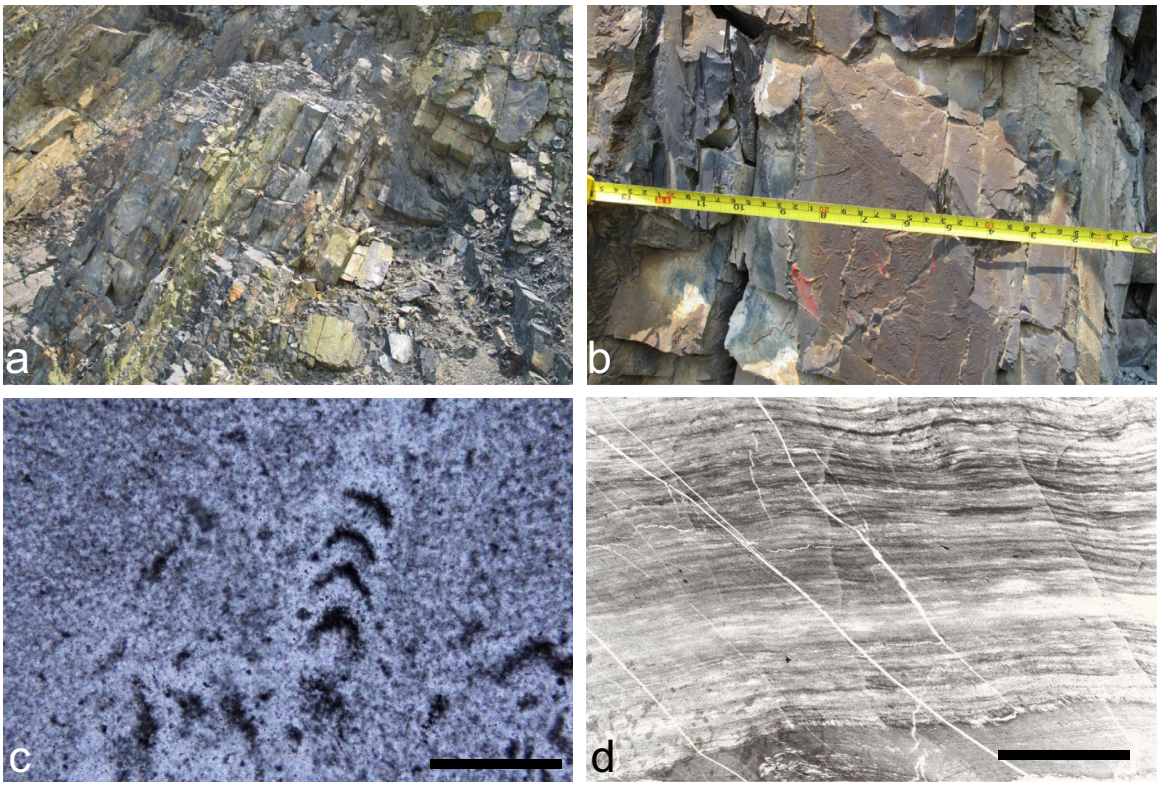

Figure 3. (a) Field photographs of the Laobao chert in the Silikou section, northern Guanxi. (b) Close view of medium bedded chert of the Laobao Formation. (c) Photomicrograph of *Palaeopascichnus* from the Laobao chert. (d) Photomicrograph of thin-laminated Laobao chert under transmitted light. Scale bars are 100 μm in Figure 3c and 2 mm in Figure 3d.

into three types (Figures 4a–4d). Type A cherts (n = 5) are characterized by high SiO_2 (average 93 wt %), low MgO + CaO (<2 wt %), and high MgO/CaO (0.5–35 with average of 9.5 (wt %/wt %)). Type B chert (n = 1) has low SiO_2 (~73 wt %), high Mg and Ca contents (MgO + CaO = 11 wt %), and low MgO/CaO (0.5). Type C cherts (n = 2) have intermediate SiO_2 (~84 wt %), MgO + CaO (3.9 wt %), and MgO/CaO (0.5–3 with an average of ~1.2), but high Al_2O_3 content (6.6 wt %). High Al_2O_3 likely reflects higher clay content, whereas high CaO reflects greater carbonate content.

The three chert types have systematic variations in Ge/Si ratios (Figure 4e). Type A cherts have the lowest Ge/Si ratio, ranging from 0.4 to 0.9 with an average of 0.6 (excluding one outlier with unusually low SiO_2 and high MgO + CaO). Type B chert with high MgO + CaO has high Ge/Si ratio of 1.5. Ge/Si ratios of Type C cherts overlap with the upper range of Type A cherts, ranging from 0.6 to 0.9 with an average value of 0.7 (excluding one outlier with very low SiO_2 but high MgO + CaO). Two measurements were made on pyrite/iron-oxide crystals identified under microscope. These iron-rich (>60% of FeO) minerals are characterized by very high Ge/Si (3.6 and 3.5).

5. Discussion

5.1. Major Element Compositions of the Laobao Cherts

The compositional difference between Type A and Type B cherts is mainly due to the presence of a greater dolomite component in Type B cherts. Stoichiometric dolomite has MgO/CaO of ~0.7 by weight. Thus, Type B cherts, with low MgO/CaO of ~0.5 but high MgO + CaO, derive their Mg and Ca contents from dolomite (Figure 4a). This is consistent with the presence of dolomite residue under microscope. In contrast, high MgO/CaO of Type A and Type C cherts implies Mg must derive from additional Mg-rich sources besides dolomite (Figure 4a). The linear correlation between MgO and Al_2O_3 in Type A cherts suggests that Mg may be associated with clays (Figure 4d). The presence of clay minerals in the Laobao chert is also supported by

Table 1. Elemental Compositions and Ge/Si of the Laobao Cherts

Sample No.	#	Na_2O (wt %)	MgO (wt %)	Al_2O_3 (wt %)	SiO_2 (wt %)	P_2O_5 (wt %)	K_2O (wt %)	CaO (wt %)	TiO_2 (wt %)	FeO (wt %)	V (ppm)	Cr (ppm)	Mn (ppm)	Co (ppm)	Ni (ppm)	Cu (ppm)	Zn (ppm)	Ga (ppm)	Ge (ppm)	Y (ppm)	Zr (ppm)	Ge/Si (μmol/mol)
Lb-29	1	0.125	0.601	3.08	93.4	0.0187	1.77	0.0693	0.309	0.553	120	426	23.6	0.993	8.18	16.4	6.73	8.49	0.918	8.63	55.1	0.795
	2	0.0434	0.482	2.91	94.3	0.0157	1.41	0.0605	0.289	0.434	141	189	21.9	1.07	9.65	36.8	14.3	7.44	0.608	27.4	37.4	0.522
	3	0.0625	0.450	2.20	95.1	0.0165	1.36	0.0128	0.145	0.568	101	245	19.2	0.865	9.55	29.9	9.39	6.43	0.573	5.08	30.1	0.488
	4	0.0743	0.411	2.17	95.2	0.0092	1.18	0.0352	0.189	0.655	105	372	27.3	0.955	7.98	22.9	11.2	6.19	0.522	2.65	21.2	0.444
	5	14.6	3.48	1.49	72.4	0.0089	0.80	6.77	0.056	0.224	9.42	220	40.8	0.580	3.57	7.04	8.10	1.90	1.109	3.59	41.4	1.24
Lb-32	1	0.104	1.02	3.58	91.0	0.156	2.41	0.543	0.261	0.841	151	797	55.6	3.03	28.7	28.3	48.2	8.98	0.930	17.0	62.4	0.827
	2	0.132	0.766	2.94	92.7	0.0334	1.94	0.0652	0.253	1.07	150	636	45.4	3.35	25.8	37.7	56.9	8.02	0.624	25.5	61.0	0.545
	3	0.0727	0.689	2.71	92.2	0.0508	1.99	0.284	0.256	1.62	136	408	55.7	5.41	22.6	55.6	28.5	5.75	0.718	7.57	30.0	0.630
	4	0.0463	0.706	2.57	93.6	0.0350	1.52	0.11	0.189	1.20	117	700	48.0	3.61	17.6	33.9	39.2	5.54	0.534	5.76	23.7	0.462
Lb-34	1	0.089	0.798	3.93	92.4	0.0183	2.15	0.0828	0.258	0.156	193	250	15.5	0.160	7.48	24.8	19.1	12.2	0.980	9.29	62.4	0.858
	2	0.077	0.751	3.82	93.0	0.0210	1.78	0.0919	0.231	0.144	204	278	10.4	0.167	8.37	27.4	19.5	11.0	0.820	6.66	53.4	0.713
	3	0.058	0.640	2.66	94.0	0.0282	1.74	0.0451	0.198	0.565	196	284	10.6	0.167	4.29	18.8	18.6	10.4	0.754	4.62	35.6	0.650
	4	0.052	0.530	2.59	94.8	0.0147	1.59	0.0281	0.233	0.110	138	206	10.5	0.120	5.48	9.46	15.5	8.06	0.628	4.07	38.7	0.536
	5	0.071	0.597	3.16	93.1	0.0930	1.82	0.0723	0.274	0.820	151	235	10.1	0.152	4.44	14.1	16.3	9.00	1.06	3.47	25.8	0.923
Lb-41	1	15.3	3.78	1.42	70.3	0.00675	0.857	7.76	0.137	0.269	14.5	180	55.2	0.678	4.01	37.3	17.2	2.67	1.66	15.0	56.9	1.91
	2	11.6	3.62	1.64	75.4	0.0101	0.687	6.59	0.102	0.208	13.9	121	47.6	0.471	4.05	37.6	25.6	1.95	1.13	20.2	69.0	1.21
	3	11.9	3.72	2.16	72.2	0.0272	0.657	8.77	0.119	0.328	14.9	468	51.2	0.560	4.71	33.9	33.6	2.49	1.10	30.0	108	1.23
Lb-46	1	1.19	1.28	7.88	85.0	0.0788	1.83	1.61	0.519	0.535	193	2326	45.3	0.633	9.45	75.7	93.2	11.0	0.835	105	130	0.795
	2	1.97	1.49	6.92	83.8	0.0996	2.06	2.18	0.352	1.00	188	2284	50.4	0.776	13.6	88.9	100	10.1	0.846	114	119	0.817
	3	1.09	1.20	6.77	85.5	0.172	2.19	1.77	0.297	0.797	159	2437	52.0	0.816	13.4	73.2	102	10.3	0.935	131	132	0.885
	4	0.974	1.19	8.08	85.2	0.0813	2.41	1.06	0.325	0.530	170	1803	38.4	0.742	11.2	70.8	80.9	10.3	0.793	103	134	0.753
Lb-49	1	0.0396	0.511	2.31	95.3	0.0111	1.39	0.0384	0.210	0.114	108	293	9.45	0.136	4.68	4.86	9.19	6.35	0.837	3.68	21.8	0.711
	2	0.0275	0.386	2.06	96.0	0.00395	1.10	0.0338	0.174	0.143	110	232	9.35	0.274	3.63	4.70	18.0	6.13	0.481	4.10	26.4	0.406
	3	0.0303	0.528	2.15	95.6	0.00661	1.26	0.0356	0.198	0.155	126	278	14.8	0.178	4.21	4.10	17.4	6.36	0.484	8.43	58.1	0.410
	4	0.0215	0.473	2.05	95.6	0.00461	1.23	0.0187	0.287	0.275	141	324	11.2	0.273	6.53	3.95	30.7	6.61	0.598	3.76	28.7	0.506
	5	0.0312	0.505	2.15	95.5	0.00637	1.27	0.0725	0.226	0.125	127	325	11.9	0.101	2.64	4.37	10.1	6.28	0.662	8.29	35.1	0.561
Lb-52	1	14.0	4.46	2.50	68.4	0.0406	1.35	8.26	0.121	0.648	66.4	742	64.7	1.14	8.79	15.4	51.8	5.28	1.01	15.0	82.5	1.20
	2	1.92	1.49	6.03	85.5	0.0385	1.62	1.96	0.340	0.940	138	362	55.5	1.64	15.7	15.6	72.0	9.65	0.640	16.6	88.1	0.606
	3	1.56	1.53	7.25	85.7	0.0389	1.70	1.12	0.428	0.585	175	444	44.3	1.54	13.3	21.6	47.9	10.1	0.701	20.4	125	0.662
	4	1.09	1.46	7.63	86.0	0.0568	1.89	0.899	0.315	0.599	157	368	79.9	2.00	14.4	22.3	46.8	9.34	0.659	14.7	84.8	0.621
	5	0.651	1.27	6.29	87.7	0.0583	1.76	0.416	0.310	1.43	156	406	102	5.52	24.2	40.5	55.4	10.5	0.618	14.2	157	0.571
Lb-57	1	0.774	0.766	3.71	92.1	0.0447	1.08	0.581	0.164	0.765	99.7	283	35.3	0.871	6.52	28.5	30.3	5.49	0.584	16.1	43.6	0.514
	2	0.653	1.10	4.53	90.5	0.0828	1.33	0.621	0.234	0.873	142	261	45.8	1.71	10.5	28.6	34.9	6.82	0.620	24.9	91.7	0.555
	3	0.244	1.02	3.79	92.1	0.0621	1.40	0.309	0.202	0.734	130	452	54.3	2.28	10.3	31.2	38.9	7.08	0.673	18.1	92.1	0.592
	4	0.215	0.660	2.47	93.4	0.0686	1.48	0.357	0.226	1.07	131	752	44.7	1.84	9.17	26.1	42.1	6.44	0.644	7.43	21.3	0.559
	5	0.145	0.658	2.27	93.8	0.169	1.48	0.316	0.203	0.896	125	485	45.8	1.38	9.78	20.8	33.6	6.34	0.589	18.1	36.1	0.508
Pyrite	1	3.86	1.09	1.94	25.4	0.433	0.637	2.577	0.036	63.8	44.8	86.1	1401	318	2080	11.0	4435	2.19	0.807	718	36.4	2.57
	2	3.46	1.16	3.45	27.9	0.375	0.641	1.63	0.118	61.0	61.3	286	1838	283	2916	26.1	4660	2.48	1.19	565	60.9	3.45

positive correlations between Al_2O_3 and $K_2O + Na_2O$ in Type A and Type C cherts (Figure 4c). This scenario is also supported by higher K_2O/Na_2O in Type A and Type C cherts because K is more strongly than Na to be incorporated into clay minerals and Na is more prone to coprecipitate with carbonate (Figure 4f).

Another discernible component in the Laobao cherts is pyrite and iron-oxides. These Fe-rich minerals may account for most of the Fe in the Laobao cherts. Pyrites are the products of H_2S reacting with Fe during bacterial sulfate reduction under anoxic conditions [*Habicht and Canfield*, 1997; *Passier et al*., 1997], whereas iron-oxides might be derived from post-depositional oxidation of pyrite. In summary, the major element composition of the Laobao cherts can be described as a mixture of four components: quartz, carbonate (mainly dolomite), clay, and pyrite/iron-oxide.

5.2. Si Source of the Laobao Cherts

Precipitation of the Laobao-Liuchapo cherts in SCB requires abundant influx of Si (Figure 1). It is unclear whether Si was directly sourced from hydrothermal fluids or seawater, the latter of which is a mixture of continental weathering and hydrothermal fluid inputs. Today, most of the Si influx into the oceans is thought to come from continental weathering because modern seawater Ge/Si is low (~0.72) [*Froelich et al*., 1985, 1992; *Mortlock and Froelich*, 1987]. In contrast, significant enrichment of Ge in hydrothermal fluids results in 1 order of magnitude higher Ge/Si than that of seawater (~11) [*Mortlock and Froelich*, 1986; *Mortlock et al*., 1993]. Thus, if we can determine the Ge/Si of end-member components in these cherts, we may be able to evaluate the relative contributions of Si to the cherts.

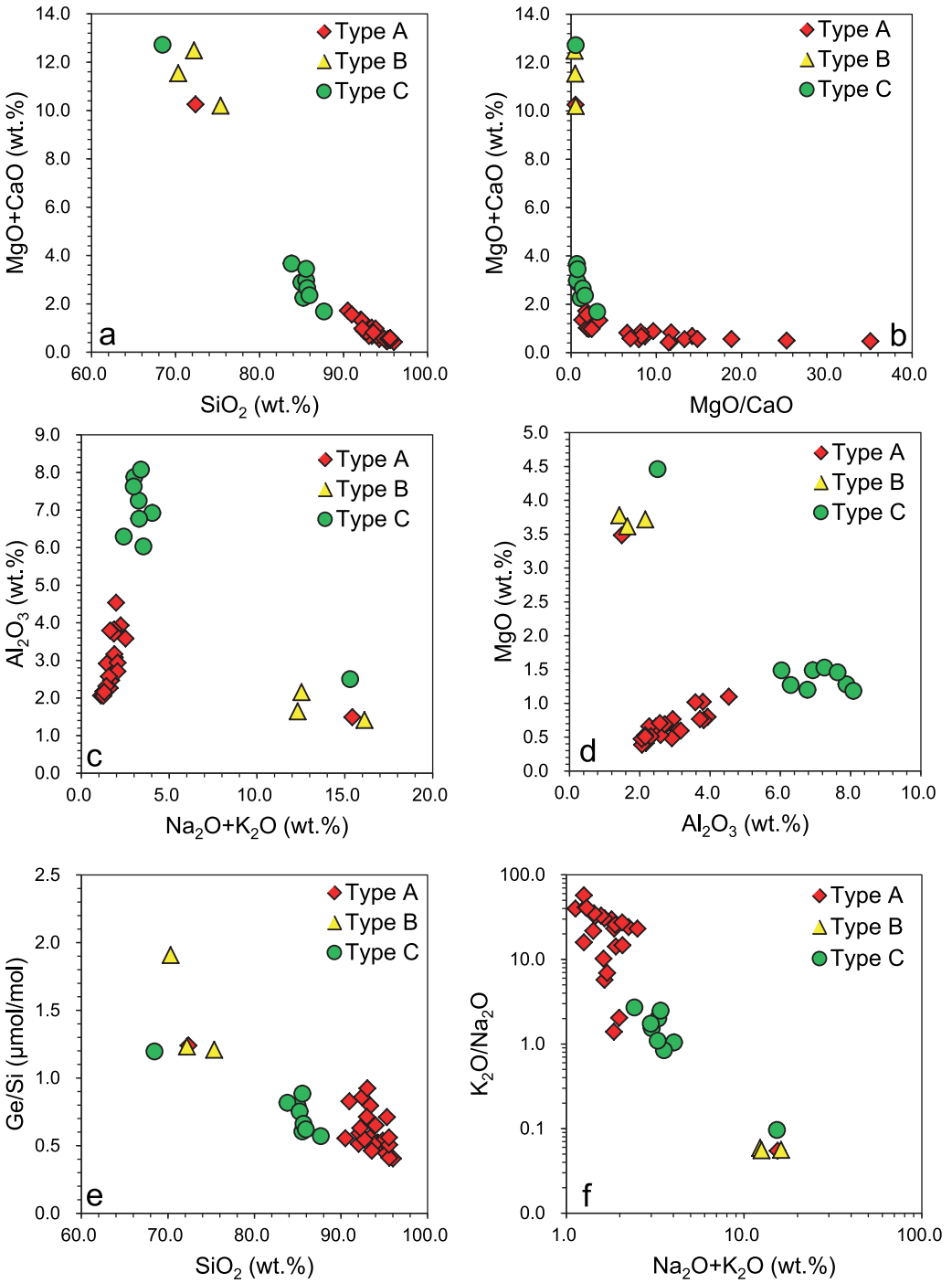

Figure 4. Cross plots showing the correlations between oxides (wt %). (a) SiO_2 versus MgO + CaO; (b) MgO + CaO versus MgO/CaO; (c) $K_2O + Na_2O$ versus Al_2O_3; (d) Al_2O_3 versus MgO; (e) SiO_2 versus Ge/Si; (f): $K_2O + Na_2O$ versus K_2O/Na_2O.

In our LA-ICP-MS methodology, our spot sizes are large enough that the bulk elemental compositions acquired are the sum of four lithological components: clay, carbonate, pyrite, and quartz. The concentration of a given element in the four different components (clay, carbonate, pyrite, and quartz) within the bulk chert is related by mass balance

$$Si_T = (x_{SiO_2} \times Si_{SiO_2} + x_{clay} \times Si_{clay}) / (x_{SiO_2} + x_{clay}) \quad (1)$$

$$Mg_T = (x_{carb} \times Mg_{carb} + x_{clay} \times Mg_{clay}) / (x_{carb} + x_{clay}) \quad (2)$$

$$Fe_T = (x_{pyrite} \times Fe_{pyrite} + x_{clay} \times Fe_{clay}) / (x_{pyrite} + x_{clay}) \quad (3)$$

where the element symbols represent the mass concentrations of a given element in each component and the bulk (where the subscripts *T*, *SiO_2*, *Clay*, *carb*, and *pyrite* denote total composition, quartz, clay, carbonate, and pyrite/iron-oxides components, respectively) and x_i is the mass fraction of component *i*.

The Ge/Si of the quartz component is estimated from the measurements with the highest SiO_2 content. It can be seen that Ge/Si is lowest (0.4–0.5) when SiO_2 is greatest (Figure 4). These values are likely maximum bounds on the Ge/Si of the quartz component in the Laobao chert for the following reasons. First, measurements with higher MgO + CaO content have significantly higher Ge/Si than those with lower MgO + CaO, suggesting that the carbonate component is characterized by high Ge/Si. Five measurements (three from Type B, one from Type A, and one from Type C cherts) with high MgO + CaO show exclusively higher Ge/Si (>1.2) than the Ge/Si of Type A and Type C cherts (0.6 and 0.7). High Ge/Si of the carbonate component cannot be attributed to the low Si content alone, because SiO_2 contents of these measurements (~70 wt %) are only 25% less than that of Type A cherts (Figure 4a). Second, clay minerals are also more enriched in Ge than the quartz component [*Kurtz et al*., 2002]. This is also evidenced by the positive correlations between Ge/Si and Al contents for most Laobao cherts samples (Figure 5). Finally, the precipitation of iron-oxide tends to absorb Ge [*Bernstein*, 1985], which may partly explain the systematic difference in Ge/Si between Si-rich and Fe-rich bands in banded iron formation [*Hamade et al*., 2003; *Maliva et al*., 2005]. Ge accumulation in iron-oxide is supported by the direct measurements of pyrite/iron-oxide particles indicating very high Ge/Si (Table 1). Therefore, incorporation of any component besides quartz will increase the Ge/Si of chert.

Our estimated Ge/Si of 0.4–0.5 of the quartz component is significantly lower than that of hydrothermal fluids [*Mortlock and Froelich*, 1986; *Mortlock et al*., 1993; *Wheat and McManus*, 2008], suggesting that hydrothermal fluids may not be the direct Si source of the Laobao cherts. Instead, Ge/Si of the quartz component is close to the modern seawater composition (0.72) [*Froelich et al*., 1985; *Hammond et al*., 2004], diatom frustules [*Murnane and Stallard*, 1988], as well as Cretaceous radiolarite that is thought to derive from dissolution-reprecipitation of siliceous radiolarian skeletons (Figure 5) [*Rouxel et al*., 2006].

In the modern ocean, the dissolved Si content of surface waters is low due to biogenic silica formation, and thus abiotic precipitation of silica directly from seawater is not possible. The only way to generate massive chert deposits, such as radiolarites, is through dissolution of biogenic silica, followed by reprecipitation of Si within sediments [*Hesse*, 1989]. However, dissolution of biogenic silica is probably not the major source of Si for the Laobao cherts during the Ediacaran-Cambrian transition, given that the dominant silica-secreting organisms in modern oceans (diatoms) did not evolve until the Mesozoic, and radiolarians and siliceous sponges may not have been ecologically important during the Ediacaran [*Racki and Cordey*, 2000; *Siever*, 1992]. Although the earliest fossil record of radiolarians probably can be traced back to the Early Cambrian [*Braun et al*., 2007; *Racki and Cordey*, 2000], they have never been abundant in Cambrian rocks. The arrival of sponges dates back into the Ediacaran and probably into the Cryogenian [*Brasier et al*., 1997; *Gehling and Rigby*, 1996; *Li et al*., 1998; *Love et al*., 2009; *Steiner*, 1994; *Zhou et al*., 1998], but despite the early appearance of sponges, it is not until the Cambrian that sponge fossils become abundant [*Rigby and Hou*, 1995; *Steiner et al*., 1993; *Zhang and Pratt*, 1994], as exemplified by abundance of sponge spicules and Burgess-shale type soft-bodied sponge fossils from the early Cambrian black shale of the Niutitang Formation in Hunan and Guizhou provinces and the equivalent Hetang Formation in Anhui province [*Xiao et al*., 2005; *Yuan et al*., 2002].

It seems likely that direct abiotic precipitation of dissolved Si from seawater, rather than dissolution/precipitation of biogenic silica produced by canonical silica-secreting organisms (e.g., radiolarian, siliceous sponge), might be one plausible mechanism for precipitating the Laobao cherts. However, abiotic silica precipitation might be facilitated by microbial activities. Recent discovery of Si-accumulation picocyanobacteria in the modern ocean indicates that such microbes can significantly enrich Si in cells, resulting in high cellular Si/P and Si/S comparable to those of diatoms [*Baines et al*., 2012].

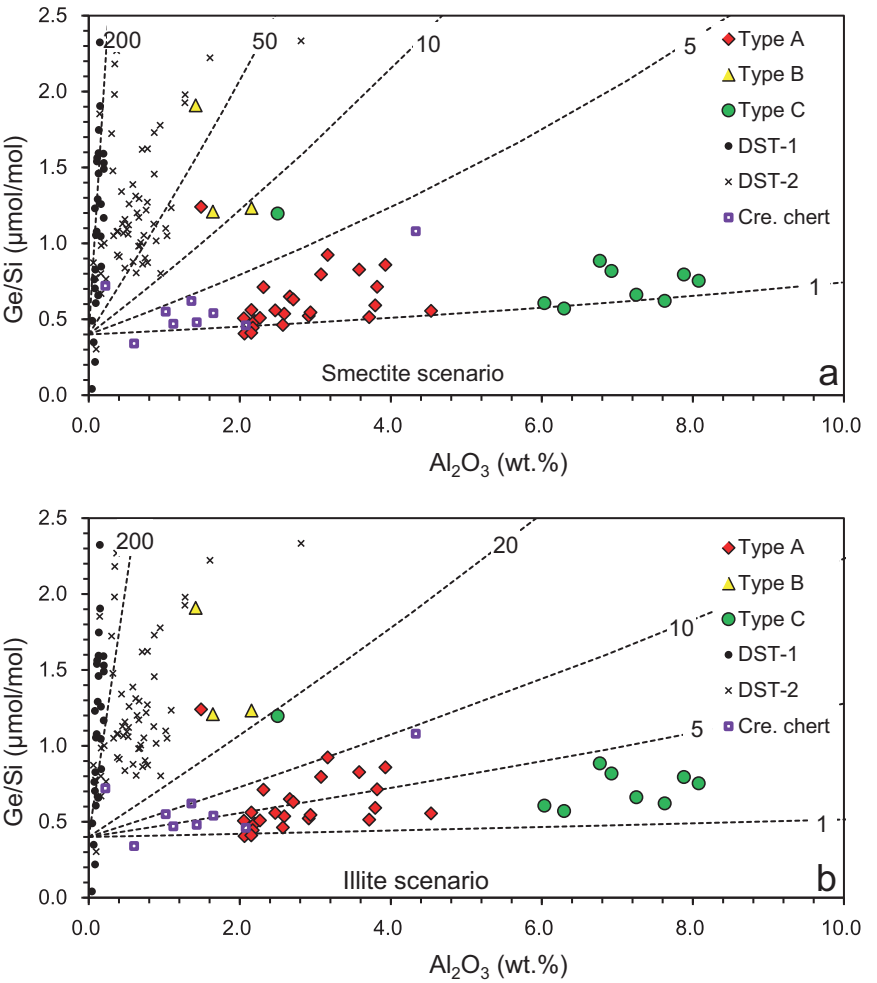

Figure 5. Cross plots showing the relationship between Al_2O_3 (wt %) and Ge/Si (μmol/mol) of the Laobao cherts, Cretaceous deep sea cherts, and Doushantuo chert nodules [*Shen et al*., 2011a]. Assuming the clay component is represented by smectite with (a) $Al_2O_3/SiO_2 = 0.25$ (wt %/wt %) and (b) illite with $Al_2O_3/SiO_2 = 0.6$. The dashed lines are binary mixing lines between the SiO_2 component and clay component with different $(Ge/Si)_{clay}$; $(Ge/Si)_{SiO_2}$ is set to 0.4. Numbers on the dashed lines represent Ge/Si of clay component. DST-1 and DST-2 are the Type I and Type II Doushantuo chert nodules from the Jiulongwan section, Yangtze Gorges area[*Shen et al*., 2011a]; "Cret. Chert" represents Cretaceous radiolarite deep sea chert [*Rouxel et al*., 2006].

5.3. Paleoenvironmental Background of Laobao Cherts Formation

In this section, we develop a model to quantify the Ge/Si systematics of the Laobao cherts. The Ge/Si ratio of bulk chert is given by:

$$(Ge/Si)_{chert} = \frac{\sum (Ge/Si)_i \times x_i \times Si_i}{\sum x_i \times Si_i} \quad i = clay, SiO_2, carb, \text{ and } pyrite \tag{4}$$

where subscripts *chert*, *clay*, SiO_2, *carb*, and *pyrite* represent bulk chert, the clay, quartz, carbonate, and pyrite components, respectively; x_i is the mass fraction of the component *i* in chert; Si_i is the SiO_2 concentration within component *i*. For Type A and C cherts, the quartz and clay components account for ~99 wt % ($SiO_2+Al_2O_3+Na_2O+K_2O+MgO = 98.9$ wt %, excluding one outlier) and ~96 wt % ($SiO_2+Al_2O_3+Na_2O+K_2O = 95.9\%$, excluding one outlier) of the total mass, so the concentrations of carbonate and pyrite within these cherts are very low. Si is also a trace element in the carbonate and pyrite components and thus their contributions to the Ge/Si systematics of the chert are negligible. The four component mixing equation can be simplified to a binary model that only considers mixing between quartz and clay components, as done by *Shen et al*. [2011a] for the Doushantuo chert nodules:

$$(Ge/Si)_{chert} = \frac{f \times (Ge/Si)_{clay} \times Si_{clay} + (1-f) \times (Ge/Si)_{SiO_2} \times Si_{SiO_2}}{f \times Si_{clay} + (1-f) \times Si_{SiO_2}} \quad (5)$$

where subscripts *chert*, *clay*, and SiO_2 denote bulk chert, the clay component, and the quartz component; f is the mass fraction of the clay component within this binary mixing system; and Si_x is the Si concentration in component x. The binary mixing model cannot completely resolve the Ge-Si systematics of Type B chert, which contains >11 (wt.%) of MgO + CaO.

Since Al only occurs in the clay component, we can use Al to represent the clay component, that is,

$$Al_{chert} = f \times Al_{clay} \quad (6)$$

The Al content in the clay component is related to clay mineral type. The most likely clay minerals in marine sediments are smectite and illite, which have Al_2O_3/SiO_2 of 0.25 and 0.6 (wt %/wt %) [*Awwiller*, 1993]. We calculate a range of f using smectite and illite end-members. To obtain the Ge/Si ratio of clay from equation (5), we assume that the Ge/Si ratio of quartz, $(Ge/Si)_{SiO_2}$, is 0.4 (wt %/wt %), corresponding to the maximum estimate of quartz Ge/Si in the Laobao cherts.

As shown in Figure 5, the Laobao cherts and the Doushantuo chert nodules plot in different regions of the Al_2O_3-Ge/Si cross plot. The estimated $(Ge/Si)_{clay}$ of the Laobao chert varies from 1 to 5 if smectite is assumed and from 1 to 10 if illite is assumed. Both numbers are within the range of Ge/Si of typical marine clays and the clay component of Cretaceous deep sea radiolarite cherts [*Bernstein*, 1985; *Kurtz et al*., 2002; *Rouxel et al*., 2006], but 1–2 orders of magnitude lower than $(Ge/Si)_{clay}$ of the early Ediacaran Doushantuo chert nodules [*Shen et al*., 2011a] (Figure 5).

The early Ediacaran Doushantuo chert nodules are interpreted to have formed in an intraplatform basinal environment, whereas the late Ediacaran-early Cambrian Laobao chert is interpreted to have deposited in a deep basinal environment. The high $(Ge/Si)_{clay}$ (ranging from 20 to 400 μmol/mol versus <10 μmol/mol in modern marine sediments) of the Doushantuo chert nodules is interpreted to reflect the presence of high DOC content in the early Ediacaran seawater [*Shen et al*., 2011a]. With high DOC content, Ge is prone to chelate with organic matter, forming Ge-Org complex [*Pokrovski and Schott*, 1998; *Pokrovski et al*., 2000], whereas Si remains in inorganic $Si(OH)_4$ form. Further absorption of Ge-Org complexes onto clay mineral surfaces results in the formation of a Ge-Org-Clay complex, enhancing the Ge/Si ratio of clay $(Ge/Si)_{clay}$.

The Laobao cherts, by contrast, have low $(Ge/Si)_{clay}$ (1–10 μmol/mol), suggesting low DOC content in late-Ediacaran seawater. We speculate that when the Laobao cherts were formed, seawater Ge was mainly in inorganic $Ge(OH)_4$ form, and remained so when incorporated into the quartz component. With the absence of Ge-Org complex in seawater, Ge in the clay component is sourced from the replacement of Si within the crystal lattice of clay mineral, not by adsorption of Ge-rich organics, thus explaining why the $(Ge/Si)_{clay}$ of the Laobao cherts is similar to that of typical marine clay minerals.

The clay Ge/Si ratios suggest that the high DOC conditions of early Ediacaran oceans did not extend into the Ediacaran-Cambrian transition. While the terminal Ediacaran deep water settings of the SCB might have been anoxic [*Chang et al*., 2012], the DOC concentration was already low enough that seawater Ge was dominated by $Ge(OH)_4$ instead of Ge-org complexes. Depletion of seawater DOC in the deep basinal environments of the SCB might be related to the possible oxidation of Ediacaran ocean, as suggested by a large negative carbon isotope excursion in the Member III of the Doushantuo Formation (the Shuram Excursion) in the Yangtze platform [*McFadden et al*., 2008; *Zhu et al*., 2013]. The negative carbon isotope excursion is interpreted as remineralization of ^{13}C-depleted DOC during the oxygenation of Ediacaran deep oceans [*Fike et al*., 2006; *Kaufman et al*., 2007; *McFadden et al*., 2008; *Shen et al*., 2011b]. If so, we speculate that the oxidation of the Ediacaran ocean was so effective that even DOC stored within deep water settings in SCB might have been oxidized. However, there is another possibility that cannot be ruled out at current time. Because the Shuram excursion is not well recorded in the slope and basinal sections [*Jiang et al*., 2007], it is possible that only the intermediate depth of water column (probably corresponding with the sulfidic wedge) is enriched in DOC [*Li et al*., 2010], whereas the deep water (probably the ferruginous zone) might be DOC poor. To further differentiate these two hypotheses, measurements of chert nodules from the deep water Doushantuo Formation or the Dengying carbonate in the shallow platform are required.

5.4. Constraints on Bedded Chert Formation

The presence of the carbonate component (Figures 4a and 4b) and the preservation of dolomite relicts and ghosts of dolomite precursors in the Laobao cherts may suggest the cherts originate from carbonate replacement [*Maliva et al*., 2005]. However, unlike most Phanerozoic carbonate-replacement cherts, which derive from dissolution and reprecipitation of biogenic silica (e.g., siliceous sponge spicules, radiolarian tests, and diatom frustules) [*Hesse*, 1989; *Maliva et al*., 2005], Ge/Si ratios suggest that normal seawater provides most of the Si for the Laobao chert formation. Furthermore, most Phanerozoic carbonate-replacement cherts are characterized by chert nodules or thin discontinuous layers within carbonate host rocks. It is less likely for carbonate-replacement cherts to form continuous bedded cherts with significant thickness (up to 100 m) and wide range of geographic distribution (more than hundreds of thousands of km^2). Carbonate-replacement origin of the Laobao chert is also not supported by the presence of centimeter-scale chert-dolomite alternations in some localities.

If carbonate replacement is not the main cause of the bedded chert formation, alternative possibilities are that the Laobao cherts precipitated directly from seawater and/or during replacement of calcareous sediments near the sediment-water interface during very early diagenesis. Both scenarios are plausible, given the high Si concentration in Precambrian seawater [*Siever*, 1992]. However, high Si content in seawater is unlikely to be the only control on Laobao chert formation, so additional factors must be considered as well.

A recent study indicates that some picocyanobacteria can accumulate Si from modern Si-poor seawater, as evident by the high cellular Si/P and Si/S ratios approaching to those of diatoms [*Baines et al*., 2012]. This finding implies that microbial activities play an important role in the modern marine Si cycle. It is well known from the fossil records that siliceous sponges and radiolarians had already evolved during late Ediacaran-early Cambrian [*Racki and Cordey*, 2000]. Thus, it is plausible that, along with the evolution of siliceous sponges and radiolarians, some bacteria might have acquired the function of Si accumulation during the Ediacaran-Cambrian transition. Possible involvement of Si-accumulation bacteria for the bedded chert formation is consistent with the widespread microbial structures/laminations seen in the Liuchapo-Laobao chert [*Hu*, 2008].

The Laobao cherts may ultimately provide new insight into the secular variation in silica diagenesis. Early diagenetic subtidal cherts are limited in Paleoproterozoic, whereas early diagenetic cherts are restricted in peritidal environments during Mesoproterozoic and Neoproterozoic [*Maliva et al*., 2005]. Early diagenetic origin of the Laobao cherts deposited in the subtidal environments implies that the reoccurrence of early diagenetic subtidal cherts during the Ediacaran-Cambrian transition, is probably due to the sudden emergence of Si-accumulation bacteria that parallels the evolution of biomineralization of silica.

6. Conclusions

The Laobao-Liuchapo bedded chert is composed of four components: quartz, carbonate, clay, and pyrite/iron-oxide components. The Ge/Si ratio of the quartz component is estimated to be 0.4–0.5 μmol/mol. This value excludes the probability of direct hydrothermal origin of Si; instead, the Si in the Laobao chert is mainly from normal seawater. $(Ge/Si)_{clay}$ of the Laobao chert is estimated ranging from 1 to 10 μmol/mol, within the range of typical marine clay minerals, but in sharp contrast to the high $(Ge/Si)_{clay}$ of the early Ediacaran Doushantuo chert nodules. We suggest that low $(Ge/Si)_{clay}$ of the Laobao chert implies low DOC concentration in the terminal Ediacaran seawater. Absence of high DOC content in the deep water environment of SCB may have resulted from massive oxidation of DOC stored in Ediacaran deep oceans during the oxidation of Ediacaran oceans. Finally, direct seawater origin of the Laobao cherts is inconsistent with the carbonate-replacement mechanism. Instead, silica precipitation in the early diagenesis might be the most likely cause. We speculate that the possible occurrence of Si-accumulation bacteria might have played a role in the Liuchapo-Laobao bedded chert formation in SCB.

Acknowledgments

The data for this paper are available by contacting with Bing Shen. Email: bingshen@pku.edu.cn. This study was supported by Natural Science Foundation of China (41402025) to Dong and (41272017 and 41322021) to Shen, Laboratory of Paleontology and Stratigraphy Open-lab grant (133103) to Dong, and a Frontiers of Earth Systems Dynamics grant from the U.S. National Science Foundation (OCE-1338842) to Lee.

References

Amthor, J. E., J. P. Grotzinger, S. Schröder, S. A. Bowring, J. Ramezani, M. W. Martin, and A. Matter (2003), Extinction of *Cloudina* and *Namacalathus* at the Precambrian-Cambrian boundary in Oman, *Geology*, *31*(5), 431–434.

Awwiller, D. N. (1993), Illite/smectite formation and potassium mass transfer during burial diagenesis of mudrocks: A study from the Texas Gulf Coast Paleocene-Eocene, *J. Sediment. Res.*, *63*(3), 501–512.

Baines, S. B., B. S. Twining, M. A. Brzezinski, J. W. Krause, S. Vogt, D. Assael, and H. McDaniel (2012), Significant silicon accumulation by marine picocyanobacteria, *Nat. Geosci.*, *5*(12), 886–891.
Bernstein, L. R. (1985), Germanium geochemistry and mineralogy, *Geochim. Cosmochim. Acta*, *49*(11), 2409–2422.
Brasier, M., O. Green, and G. Shields (1997), Ediacarian sponge spicule clusters from southwestern Mongolia and the origins of the Cambrian fauna, *Geology*, *25*(4), 303–306.
Braun, A., J. Chen, D. Waloszek, and A. Maas (2007), First Early Cambrian Radiolaria, *Geol. Soc. Spec. Publ.*, *286*(1), 143–149.
Chang, H.-J., X.-L. Chu, L.-J. Feng, J. Huang, and Q.-R. Zhang (2008), REE geochemistry of the Liuchapo chert in Anhua, Hunan, *Chin. Geol.*, *35*, 879–887.
Chang, H.-J., X.-L. Chu, L.-J. Feng, J. Huang, and Q.-R. Zhang (2010), The Major and REE geochemistry of the Silikou Chert in Northern Guangxi province, *Acta Sedimentol. Sinica*, *28*, 1098–1107.
Chang, H.-J., X.-L. Chu, L.-J. Feng, and J. Huang (2012), Progressive oxidation of anoxic and ferruginous deep-water during deposition of the terminal Ediacaran Laobao Formation in South China, *Palaeogeogr. Palaeoclimatol. Palaeoecol.*, *321–322*, 80–87.
Chen, D., X. Zhou, Y. Fu, J. Wang, and D. Yan (2015), New U–Pb zircon ages of the Ediacaran–Cambrian boundary strata in South China, *Terra Nova*, *27*, 62–68, doi:10.1111/ter.12134.
Condon, D., M. Zhu, S. Bowring, W. Wang, A. Yang, and Y. Jin (2005), U-Pb ages from the Neoproterozoic Doushantuo Formation, China, *Science*, *308*, 95–98.
De Argollo, R., and J. G. Schilling (1978), Ge/Si and Ga/Al fractionation in Hawaiian volcanic rocks, *Geochim. Cosmochim. Acta*, *42*(6, Part A), 623–630.
Dong, L., S. Xiao, B. Shen, and C. Zhou (2008), Silicified Horodyskia and Palaeopascichnus from upper Ediacaran cherts in South China: Tentative phylogenetic interpretation and implications for evolutionary stasis, *J. Geol. Soc.*, *165*, 367–378.
Dong, L., W. Song, S. Xiao, X. Yuan, Z. Chen, and C. Zhou (2012), Micro- and macrofossils from the Piyuancun Formation and their implications for the Ediacaran-Cambrian boundary in Southern Anhui, *J. Stratigr.*, *36*, 600–610.
Fan, H., H. Wen, X. Zhu, R. Hu, and S. Tian (2013), Hydrothermal activity during Ediacaran–Cambrian transition: Silicon isotopic evidence, *Precambrian Res.*, *224*, 23–35.
Fike, D. A., J. P. Grotzinger, L. M. Pratt, and R. E. Summons (2006), Oxidation of the Ediacaran ocean, *Nature*, *444*, 744–747.
Froelich, P. N., G. A. Hambrick, M. O. Andreae, R. A. Mortlock, and J. M. Edmond (1985), The geochemistry of inorganic germanium in natural waters, *J. Geophys. Res.*, *90*, 1133–1141, doi.10.1029/JC090iC01p01133.
Froelich, P. N., R. A. Mortlock, and A. Shemesh (1989), Inorganic germanium and silica in the Indian Ocean: Biological fractionation during (Ge/Si) opal formation, *Global Biogeochem. Cycles*, *3*, 79–88, doi:10.1029/GB003i001p00079.
Froelich, P. N., V. Blanc, R. A. Mortlock, S. N. Chillrud, W. Dunstan, A. Udomkit, and T. H. Peng (1992), River fluxes of dissolved silica to the ocean were higher during glacials: Ge/Si In diatoms, rivers, and oceans, *Paleoceanography*, *7*, 739–767, doi:10.1029/92PA02090.
Gehling, J. G., and J. K. Rigby (1996), Long expected sponges from the Neoproterozoic Ediacara fauna of South Australia, *J. Paleontol.*, *70*(2), 185–195.
Habicht, K. S., and D. E. Canfield (1997), Sulfur isotope fractionation during bacterial sulfate reduction in organic-rich sediments, *Geochim. Cosmochim. Acta*, *61*, 5351–5361.
Hamade, T., K. O. Konhauser, R. Raiswell, S. Goldsmith, and R. C. Morris (2003), Using Ge/Si ratios to decouple iron and silica fluxes in Precambrian banded iron formations, *Geology*, *31*(1), 35–38.
Hammond, D. E., J. McManus, and W. M. Berelson (2004), Oceanic germanium/silicon ratios: Evaluation of the potential overprint of temperature on weathering signals, *Paleoceanography*, *19*, PA2016, doi:10.1029/2003PA000940.
Hesse, R. (1989), Silica diagenesis: Origin of inorganic and replacement cherts, *Earth Sci. Rev.*, *26*, 253–284.
Hu, J. (2008), The cherty microbolite in the deeper water facies during the Precambrian-Cambrian transional period in northeast Guangxi province, China, *Acta Mineral. Sinica*, *25*, 291–305.
Jiang, G., A. J. Kaufman, N. Christie-Blick, S. Zhang, and H. Wu (2007), Carbon isotope variability across the Ediacaran Yangtze platform in South China: Implications for a large surface-to-deep ocean $\delta^{13}C$ gradient, *Earth Planet. Sci. Lett.*, *261*(1-2), 303–320.
Jiang, G., X. Shi, S. Zhang, Y. Wang, and S. Xiao (2011), Stratigraphy and paleogeography of the Ediacaran Doushantuo Formation (ca. 635–551 Ma) in South China, *Gondwana Res.*, *19*, 831–849.
Kaufman, A. J., F. A. Corsetti, and M. A. Varni (2007), The effect of rising atmospheric oxygen on carbon and sulfur isotope anomalies in the Neoproterozoic Johnnie Formation, Death Valley, USA, *Chem. Geol.*, *237*, 47–63.
Knoll, A. H. (1996), Breathing room for early animals, *Nature*, *382*, 111–112.
Kolodny, Y., and L. Halicz (1988), The geochemistry of germanium in deep-sea cherts, *Geochim. Cosmochim. Acta*, *52*(9), 2333–2336.
Kurtz, A. C., L. A. Derry, and O. A. Chadwick (2002), Germanium-silicon fractionation in the weathering environment, *Geochim. Cosmochim. Acta*, *66*, 1525–1537.
Li, C., G. D. Love, T. W. Lyons, D. A. Fike, A. L. Sessions, and X. Chu (2010), A stratified redox model for the Ediacaran ocean, *Science*, *328*(5974), 80–83.
Li, C.-W., J.-Y. Chen, and T.-E. Hua (1998), Precambrian sponges with cellular structures, *Science*, *279*, 879–882.
Love, G. D., et al. (2009), Fossil steroids record the appearance of Demospongiae during the Cryogenian period, *Nature*, *457*(7230), 718–721.
Lyons, T. W., C. T. Reinhard, and N. J. Planavsky (2014), The rise of oxygen in Earth/'s early ocean and atmosphere, *Nature*, *506*(7488), 307–315.
Maliva, R. G., A. H. Knoll, and B. M. Simonson (2005), Secular change in the Precambrian silica cycle: Insights from chert petrology, *Geol. Soc. Am. Bull.*, *117*(7), 835–845.
McFadden, K. A., J. Huang, X. Chu, G. Jiang, A. J. Kaufman, C. Zhou, X. Yuan, and S. Xiao (2008), Pulsed oxidation and biological evolution in the Ediacaran Doushantuo Formation, *Proc. Natl. Acad. Sci. U. S. A.*, *105*, 3197–3202.
Mortlock, R. A., and P. N. Froelich (1986), Hydrothermal germanium over the southern East Pacific Rise, *Science*, *231*(4733), 43–45.
Mortlock, R. A., and P. N. Froelich (1987), Continental weathering of germanium: In the global river discharge, *Geochim. Cosmochim. Acta*, *51*(8), 2075–2082.
Mortlock, R. A., P. N. Froelich, R. A. Feely, G. J. Massoth, D. A. Butterfield, and J. E. Lupton (1993), Silica and germanium in Pacific Ocean hydrothermal vents and plumes, *Earth Planet. Sci. Lett.*, *119*(3), 365–378.
Murnane, R. J., and R. F. Stallard (1988), Germanium/Silicon fractionation during biogenic opal formation, *Paleoceanography*, *3*, 461–469, doi:10.1029/PA003i004p00461.
Passier, H. F., J. J. Middelburg, G. J. de Lange, and M. E. Boettcher (1997), Pyrite contents, microtextures, and sulfur isotopes in relation to formation of the youngest eastern Mediterranean sapropel, *Geology*, *25*(6), 519–522.

Peng, J., W. Xia, and H. Yi (1999), Geochemical characteristics and depositional environments of the Late Precambrian bedded siliceous rocks in western Hunan, *Sediment. Facies Palaeogeogr.*, *19*, 29–37.
Planavsky, N. J., C. T. Reinhard, X. Wang, D. Thomson, P. McGoldrick, R. H. Rainbird, T. Johnson, W. W. Fischer, and T. W. Lyons (2014), Low mid-Proterozoic atmospheric oxygen levels and the delayed rise of animals, *Science*, *346*(6209), 635–638.
Pokrovski, G. S., and J. Schott (1998), Experimental study of the complexation of silicon and germanium with aqueous organic species: Implications for germanium and silicon transport and Ge/Si ratio in natural waters, *Geochim. Cosmochim. Acta*, *62*(21–22), 3413–3428.
Pokrovski, G. S., F. Martin, J.-L. Hazemann, and S. Jacques (2000), An X-ray absorption fine structure spectroscopy study of germanium-organic ligand complexes in aqueous solution, *Chem. Geol.*, *163*(1-4), 151–165.
Racki, G., and F. Cordey (2000), Radiolarian palaeoecology and radiolarites: Is the present the key to the past?, *Earth Sci. Rev.*, *52*(1-3), 83–120.
Reinhard, C. T., N. J. Planavsky, L. J. Robbins, C. A. Partin, B. C. Gill, S. V. Lalonde, A. Bekker, K. O. Konhauser, and T. W. Lyons (2013), Proterozoic ocean redox and biogeochemical stasis, *Proc. Natl. Acad. Sci. U. S. A.*, *110*(14), 5357–5362.
Rigby, J. K., and X. Hou (1995), Lower Cambrian demosponges and hexactinellid sponges from Yunnan,China, *J. Paleontol.*, *69*, 1009–1019.
Rothman, D. H., J. M. Hayes, and R. E. Summons (2003), Dynamics of the Neoproterozoic carbon cycle, *Proc. Natl. Acad. Sci. U. S. A.*, *100*, 8124–8129.
Rouxel, O., A. Galy, and H. Elderfield (2006), Germanium isotopic variations in igneous rocks and marine sediments, *Geochim. Cosmochim. Acta*, *70*(13), 3387–3400.
Rudnick, R. L., and S. Gao (2003), Composition of the continental crust, in *The Crust*, edited by R. L. Rudnick, pp. 1–64, Elsevier, Oxford, U. K.
Shen, B., C.-T. A. Lee, and S. Xiao (2011a), Germanium/silica ratios in diagenetic chert nodules from the Ediacaran Doushantuo Formation, South China, *Chem. Geol.*, *280*(3–4), 323–335.
Shen, B., S. Xiao, H. Bao, A. J. Kaufman, C. Zhou, and X. Yuan (2011b), Carbon, sulfur, and oxygen isotope evidence for a strong depth gradient and oceanic oxidation after the Ediacaran Hankalchough glaciation, *Geochim. Cosmochim. Acta*, *75*(5), 1357–1373.
Shields-Zhou, G., and L. Och (2011), The case for a Neoproterozoic Oxygenation Event: Geochemical evidence and biological consequences, *GSA Today*, *21*(3), 4–11.
Shu, D. (2008), Cambrian explosion: Birth of tree of animals, *Gondwana Res.*, *14*(1-2), 219–240.
Siever, R. (1992), The silica cycle in the Precambrian, *Geochim. Cosmochim. Acta*, *56*(8), 3265–3272.
Steiner, M. (1994), Die neoproterozoischen Megaalgen Südchinas, *Berl. Geowissenschaftliche Abh. E*, *15*, 1–146.
Steiner, M., D. Mehl, J. Reitner, and B.-D. Erdtmann (1993), Oldest entirely preserved sponges and other fossils from the lowermost Cambrian and a new facies reconstruction of the Yangtze Platform (China), *Berl. Geowissenschaftliche Abh. E*, *9*, 293–329.
Tréguer, P., D. M. Nelson, A. J. Van Bennekom, D. J. DeMaster, A. Leynaert, and B. Quéguiner (1995), The silica balance in the world ocean: A reestimate, *Science*, *268*(5209), 375–379.
Wang, J., and Z.-X. Li (2003), History of Neoproterozoic rift basins in South China: Implications for Rodinia break-up, *Precambrian Res.*, *122*(1-4), 141–158.
Wang, J., D. Chen, D. Yan, H. Wei, and L. Xiang (2012a), Evolution from an anoxic to oxic deep ocean during the Ediacaran–Cambrian transition and implications for bioradiation, *Chem. Geol.*, *306–307*, 129–138.
Wang, J., D. Chen, D. A. N. Wang, D. Yan, X. Zhou, and Q. Wang (2012b), Petrology and geochemistry of chert on the marginal zone of Yangtze Platform, western Hunan, South China, during the Ediacaran–Cambrian transition, *Sedimentology*, *59*(3), 809–829.
Wang, Y., Y. Chen, R. Wang, X. Chen, and X. Wei (1980), Stratigraphic types and characteristics of Sinian in Hunan, Guizhou and Guangsi, in *Research in Precambrian Geology: Sinian Suberathem in China*, edited by Tianjin Institute of Geology and Mineral Resources, pp. 146–163, Tianjin Sci. and Technol. Press, Tianjin, China.
Wang, Y., G. Yin, S. Zheng, and Y. Qian (1984a), Stratigraphy of the boundary Sinian—Cambrian in the Yangzi area of Guizhou, in *The Upper Precambrian and Sinian-Cambrian Boundary in Guizhou*, edited by Y. Wang et al., pp. 1–31, People's Publ. House of Guizhou, Guiyang, China.
Wang, Y., G. Yin, S. Zheng, S. Qing, S. Zhu, Y. Chen, Q. Luo, F. Wang, and Y. Qian (1984b), *The Upper Precambrian and Sinian-Cambrian Boundary in Guizhou*, 170 pp., People's Publ. House of Guizhou, Guiyang, China.
Wang, Y., Z. Huang, H. Chen, M. Hou, Y. Yang, and B. Du (2012c), Stratigraphical correlation of the Liuchapo Formation with the Dengying Formation in South China, *J. Jilin Univ. (Earth Science Edition)*, *42*, 328–335.
Wheat, C. G., and J. McManus (2008), Germanium in mid-ocean ridge flank hydrothermal fluids, *Geochem. Geophys. Geosyst.*, *9*, Q03025, doi:10.1029/2007GC001892.
Xiao, S., J. Hu, X. Yuan, R. L. Parsley, and R. Cao (2005), Articulated sponges from the Lower Cambrian Hetang Formation in southern Anhui, South China: Their age and implications for the early evolution of sponges, *Palaeogeogr. Palaeoclimatol. Palaeoecol.*, *220*(1-2), 89–117.
Yang, E.-l., C. Hen-shui, H. Chen, W. Bo, C. Yu, Y. You, and L. Jian-jun (2011), Elemental geochemistry and sedimentary environment of the Liuchapo Siliceous rocks in Songtao-Cengong-Sandu, Eastern Guizhou province, *Acta Mineral. Sinica*, *31*, 406–411.
Yuan, X., S. Xiao, R. L. Parsley, C. Zhou, Z. Chen, and J. Hu (2002), Towering sponges in an Early Cambrian Lagerstätte: Disparity between non-bilaterian and bilaterian epifaunal tiers during the Neoproterozoic-Cambrian transition, *Geology*, *30*(4), 363–366.
Zhang, X., and B. R. Pratt (1994), New and extraordinary Early Cambrian sponge spicule assemblage from China, *Geology*, *22*, 43–44.
Zhao, G. (1999), The influence of biogenic procession on the accumulation and precipitation of silica-An example from south of Anhui and west of Zhejiang, *Acta Sedimentol. Sinica*, *17*, 30–37.
Zhou, C., X. Yuan, and Y. Xue (1998), Sponge spicule-like pseudofossils frm the Neoproterozoic Doushantuo Formation in Weng'an, Guizhou, China, *Acta Micropalaeontol. Sinica*, *15*(4), 380–384.
Zhu, M., M. Lu, J. Zhang, F. Zhao, G. Li, Y. Aihua, X. Zhao, and M. Zhao (2013), Carbon isotope chemostratigraphy and sedimentary facies evolution of the Ediacaran Doushantuo Formation in western Hubei, South China, *Precambrian Res.*, *225*, 7–28.